Force Feedback is Noticeably Different for Linear versus Nonlinear Elastic Tissue Models

Sarthak Misra, Allison M. Okamura, and K. T. Ramesh
Department of Mechanical Engineering, The Johns Hopkins University
Baltimore, MD 21218 USA
{sarthak,aokamura,ramesh}@jhu.edu

Abstract

Realistic modeling of the interaction between surgical instruments and human organs has been recognized as a key requirement in the development of high-fidelity surgical simulators. Primarily due to computational considerations, most of the past simulation research within the haptics community has assumed linear elastic behavior for modeling tissues, even though human soft tissues generally possess nonlinear viscoelastic properties. Hence, this paper quantitatively compares linear and nonlinear elasticity-based models. It is demonstrated that, for a nonlinear model, the well-known Poynting effect developed during shearing of the tissue results in normal forces not seen in a linear elastic model. The difference in force magnitude and force direction for linear and nonlinear models are larger than the just noticeable difference for contact force and force-direction discrimination thresholds published in the psychophysics literature, respectively. This work applies a proposed framework for examining the effect of tool-tissue interaction modeling techniques on human perception of surgical simulators with haptic feedback.

1. Introduction

Surgical simulators present an efficient, safe, realistic, and ethical method for surgical training, practice, and preoperative planning. Surgical simulation emphasizes the user's real-time interaction with medical instruments, surgical techniques, and realistic organ models that are anatomically and physiologically accurate. In order to further enhance the realism, some surgical simulators also have the capability to provide haptic feedback to the user. The development of realistic surgical simulation systems requires accurate modeling of the organs and their interactions with the surgical tools. The benefits of tissue modeling are not only evident for training, planning, and practice of surgical procedures, but also for optimizing surgical tool design, creating "smart" instruments capable of assessing pathology or force-limiting novice surgeons, and for understanding tissue injury mechanisms and damage thresholds.

Human organs in general are inhomogeneous, anisotropic, and exhibit nonlinear viscoelastic properties. Continuum mechanics provides a mathematical framework to model the constitutive laws of biological tissues. Though linear elastic models are frequently used to model tissues for simulating surgical procedures, such models are only accurate for materials undergoing small strains, while most surgical procedures involve organs being subjected to large strains. The behavior of materials undergoing large strains ($>$1%-2%) is described by the theory of nonlinear elasticity, e.g. hyperelastic models.

Given the complexity of human organs and challenges in acquisition of tissue parameters, realistic modeling and simulation of tissue deformation is an ongoing research area. Extensive work has been done by researchers in the area of computer graphics to model deformable bodies [5]. In such studies, the focus has been to produce seemingly realistic visualization, while ignoring the physics underlying tissue deformation. The purpose of the literature in the domain of biomechanics is understanding the fundamental properties of various tissues, e.g. [4, 26]. Within the robotics and haptics research communities, most of the past research has generally assumed linear elasticity for modeling tissues for both invasive and non-invasive surgical procedures. Examples of modeling and simulation of non-invasive surgical operations generally involve deformation via indentation, e.g. [1, 12, 14, 18] purely via simulation, or comparing simulation results with experiments on real or phantom tissues [17, 22]. Needle insertion [3] and cutting [19, 25] have been used in models of invasive surgical procedures. Some studies use a hyperelastic formulation for simulation of non-invasive surgical procedures [7, 13, 16, 24], and two studies have used a hyperelastic formulation to simulate invasive procedures [9, 20]. Further, several researchers have investigated a wide variety of methods for modeling tool-tissue interactions based on techniques other than continuum mechanics, e.g. [8, 15, 23]. The primary reason for using such non-physical modeling techniques is computational efficiency.

In this paper, we demonstrate that there is a significant difference between the forces applied to the user for lin-

Second Joint EuroHaptics Conference and Symposium on Haptic Interfaces for Virtual Environment and Teleoperator Systems (WHC'07)
0-7695-2738-8/07 $20.00 © 2007 IEEE

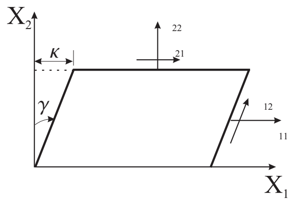

Figure 1. Body undergoing simple shear; the shear strain is κ in the X_1 direction.

ear and nonlinear elastic tissue models. While this is not a new concept, our work provides a concrete example of how modeling techniques relate to human perception of surgical simulators. We quantitatively compare both the magnitude and direction of force resulting from linear and nonlinear models, and show that these differences are far beyond the published thresholds of human sensing. For the purposes of comparison in this study, we have considered the organ to undergo shear. Shear displacement is used because, during invasive and non-invasive medical procedures, it is common practice for clinicians to palpate and perform a shearing motion on the organ either by hand or with an instrument. Deghan and Salcudean also recently compared the effects of linear and nonlinear FE models on the mesh displacement during needle insertion [2]. They concluded that in the presence of asymmetric boundary conditions, there are noticeable differences between linear and nonlinear models.

The derivations for the constitutive law of a body undergoing shear are presented in Section 2. In order to populate our model with realistic material properties, we conducted uniaxial compression tests on gel samples, as described in Section 3. Simulation studies to compare linear and nonlinear models are presented in Section 4. Finally, we discuss the implications of our results for haptic feedback in surgical simulators and potential future work.

2. Continuum mechanics-based formulation for simple shear

In order to highlight the differences between linear and nonlinear-elasticity based tissue models, this section presents the theoretical relationships for the stresses and strains for a body undergoing simple shear, as shown in Figure 1. The formulation highlights only the key relationships and does not cover the fundamentals of continuum mechanics. For further details, we refer the reader to [6].

The body is assumed to shear by an amount κ, and γ is the angle the sheared line makes with its original orientation. The shear strain is given by $\kappa = \tan(\gamma)$. If $\mathbf{y}$ represents the position after deformation of a material reference initially located at $\mathbf{X}$, we can describe the simple shear motion by

$$\mathbf{y} = (X_1 + \kappa X_2)\,\mathbf{e}_1 + X_2\mathbf{e}_2 + X_3\mathbf{e}_3, \tag{1}$$

where $\{\mathbf{e}_1, \mathbf{e}_2, \mathbf{e}_3\}$ are the Cartesian base vectors. The above expression implies that shear displacement is being applied to the body, while preventing displacement in the normal direction. From (1), the matrix of the deformation gradient tensor, $\mathbf{F}$, is computed as

$$\mathbf{F} = \frac{\partial \mathbf{y}}{\partial \mathbf{X}} = \begin{bmatrix} 1 & \kappa & 0 \\ 0 & 1 & 0 \\ 0 & 0 & 1 \end{bmatrix}. \tag{2}$$

The deformation of materials under large strains (>1%-2%) is described by the theory of nonlinear elasticity, and hyperelastic models are commonly used. For a hyperelastic material, the Cauchy stress tensor, $\boldsymbol{\sigma}$, can be derived from a strain energy density function, W [6]. There are various formulations for the strain energy density function depending on the material, e.g. Neo-Hookean, Mooney-Rivlin, St. Venant-Kirchhoff, Blatz-Ko, Ogden, and polynomial forms.

Using the Representation Theorem, the Cauchy stress tensor for an isotropic, homogenous, and incompressible hyperelastic material can be derived as [6]

$$\boldsymbol{\sigma} = -p\mathbf{I} + 2\left\{\left(\frac{\partial W}{\partial I_1} + I_1\frac{\partial W}{\partial I_2}\right)\mathbf{B} - \frac{\partial W}{\partial I_2}\mathbf{B}^2\right\}, \tag{3}$$

where I_1 and I_2 are the principal invariants, $\mathbf{B}$ is the left Cauchy-Green tensor, and p is the Lagrange multiplier (essentially a pressure). $\mathbf{B}$ is given in terms of the deformation gradient tensor as

$$\mathbf{B} = \mathbf{F}\mathbf{F}^T = \begin{bmatrix} 1+\kappa^2 & \kappa & 0 \\ \kappa & 1 & 0 \\ 0 & 0 & 1 \end{bmatrix}. \tag{4}$$

Several strain energy density functions were implemented for this study, but we present results only for the Mooney-Rivlin model, since this is sufficient to highlight the differences between linear and nonlinear models. The Mooney-Rivlin strain energy density function is given by

$$W = C_1\,(I_1 - 3) + C_2\,(I_2 - 3)\,, \tag{5}$$

where C_1 and C_2 are material parameters specific to the tissue. In (5), the principal invariants, I_1 and I_2, can be evaluated from $\mathbf{B}$ as

$$I_1 = \mathbf{B} : \mathbf{I} \text{ and } I_2 = \frac{1}{2}\Big((\mathbf{B}:\mathbf{I})^2 - (\mathbf{B}:\mathbf{B})\Big). \tag{6}$$

Thus,

$$I_1 = \kappa^2 + 3 \text{ and } I_2 = \kappa^2 + 3. \tag{7}$$

Further, for the Mooney-Rivlin model given in (5)

$$\frac{\partial W}{\partial I_1} = C_1 \text{ and } \frac{\partial W}{\partial I_2} = C_2. \tag{8}$$

From (4), we can compute $\mathbf{B}^2$, and using results from (7) and (8), and evaluating (3), we obtain the following expres-

Second Joint EuroHaptics Conference and Symposium on Haptic
Interfaces for Virtual Environment and Teleoperator Systems (WHC'07)
0-7695-2738-8/07 $20.00 © 2007 IEEE

sions for the stress in terms of the shear, κ:

$$\sigma_{11} = 2C_1 + 4C_2 + 2\left(C_1 + C_2\right)\kappa^2 - p \tag{9}$$

$$\sigma_{22} = 2C_1 + 4C_2 - p \tag{10}$$

$$\sigma_{33} = 2C_1 + 2C_2\left(2 + \kappa^2\right) - p \tag{11}$$

$$\sigma_{12} = 2\left(C_1 + C_2\right)\kappa \tag{12}$$

$$\sigma_{13} = 0 \tag{13}$$

$$\sigma_{23} = 0 \tag{14}$$

The Lagrange multiplier, p, can be evaluated from the boundary condition. For example, the plane stress case gives

$$\sigma_{33} = 0 \Rightarrow p = 2\left(C_1 + 2C_2 + C_2\kappa^2\right) \tag{15}$$

As seen in (10), σ_{22} is non-zero. The presence of normal stress, σ_{22}, and the inequality, $\sigma_{11} \neq \sigma_{22}$ is a manifestation of the "Poynting effect", and is a result of the nonlinearity.

In contrast, for a homogenous and isotropic body undergoing simple shear, the stress based on linear elasticity is

$$\sigma_{12} = G\kappa, \tag{16}$$

where G is the shear modulus, and all other components of stress are zero. (16) presents a computationally simple and easy to implement formulation, but such models do not exhibit the Poynting effect.

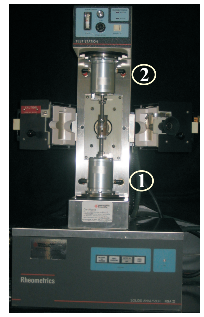

(a)

(b)

Figure 2. (a) The RSA II test station, where ① and ② are the actuator and load cell, respectively (b) The Sylgard 527 gel sample in the RSA II.

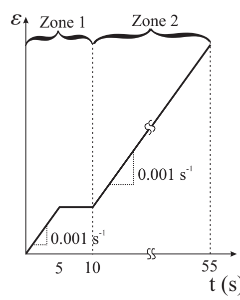

Figure 3. Strain rate sweep mode

3. Experiments to measure phantom tissue properties

In order to populate (9)-(16) with soft tissue parameters, we conducted experiments to acquire the material coefficients, C_1, C_2, and G. For a specific tissue-like material, experiments were performed on the Rheometrics Solids Analyzer (RSA) II. Dow Corning Sylgard 527 A & B silicone dielectric gel was used to simulate soft tissues. Details pertaining to the individual components and various test modes can be found in the RSA II owner's manual [21]. Sylgard 527 gel is commonly used to simulate human brain tissue. This section describes the experimental method used in order to acquire the material properties of the Sylgard 527 gel.

3.1. Methods

The Sylgard 527 gel sample to be tested was placed between the actuator and load cell, which are located on the RSA II test station, as shown in Figures 2(a) and (b). The actuator and load cell are physically identical. The position sensor mounted onto the actuator shaft outputs a DC voltage that is proportional to the actuator displacement. The resolution of the actuator is $\pm$ 0.05 μm. The load cell is operated by using a linear variable differential transducer (LVDT) in order to maintain constant axial position during testing. Following the application of force to the load cell shaft, the LVDT outputs a DC voltage that is proportional to shaft displacement from zero position. The resolution of the load cell is $\pm$ 0.00981 N.

20 Sylgard 527 gel samples of dimensions 10 mm $\times$ 10 mm and 1 mm thick were prepared and tested. For our experiments we operated the RSA II in the "strain rate sweep" mode. In this mode, the user commands a compressive strain rate and a period for which the strain is to be applied. For our tests, we applied the strains histories shown in Figure 3. During Zone 1, the initial compressive strain was applied for a period of 5 seconds and then the sample was allowed to settle for a period of 5 seconds. The data to be analyzed is from Zone 2, where the compressive strain was applied for a period of 45 seconds. Zone 1 ensures that the sample is appropriately preconditioned so that reliable stress and strain data is acquired. During both zones, the strain rate was set to 0.001 sec^{-1}.

3.2. Results

In order to obtain the material properties corresponding to the Mooney-Rivlin strain energy density function in (5), we derived the constitutive law for uniaxial compression. Using (3), in terms of the stretch ratio, λ, and the material

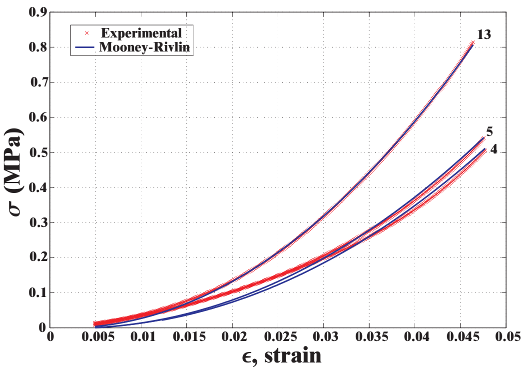

Figure 4. Experimental results and derived models based on Mooney-Rivlin strain energy density function for 3 samples.

constants, the stress is given as

$$\sigma = \frac{2\left(C_2 + C_1\lambda\right)\left(\lambda^3 - 1\right)}{\lambda^2}, \tag{17}$$

where the strain, ε, in terms of the stretch ratio is

$$\lambda = 1 - \varepsilon. \tag{18}$$

The analytical expression in (17), along with the constraint $C_1 + C_2 > 0$, was used to fit the experimental data in order to obtain the material parameters. The constraint is obtained from (12) in order to ensure appropriate direction of stress for a given strain. In order to obtain the Young's modulus, E, the experimental data was also fitted to the linear elastic model, $\sigma = E\varepsilon$. Table 1 provides the Mooney-Rivlin material coefficients and Young's modulus for 3 representative cases out of the total 20 tested samples. In Figure 4, experimental and derived stress-strain curves based on the Mooney-Rivlin parameters in Table 1 are plotted.

Table 1. Mooney-Rivlin material coefficients and Young's modulus for 3 samples of Sylgard 527 derived for experimental stress-strain curves (representative data out of the total 20 samples).

Sample #	C_1 (MPa)	C_2 (MPa)	E (MPa)
4	39.777	-39.579	7.880
5	42.172	-41.975	8.365
13	63.795	-63.597	12.772

4. Comparison of linear and nonlinear finite element models

In order to quantify the responses of linear and nonlinear elastic models for a specific geometry, we built a 2-D finite element (FE) model in ABAQUS (ABAQUS Inc., Providence, RI). The dimensions of the model were 15 cm × 5 cm, and the material was considered to be homogenous, isotropic, and incompressible. The model was meshed using 8-node biquadratic plane stress quadrilaterals with nodes that were 1 mm apart. For the purposes of demonstrating the Poynting effect, the Mooney-Rivlin parameters corresponding to sample #5 in Table 1 were chosen. For the linear elastic case, the shear modulus was obtained from the Young's modulus corresponding to sample #5, which is given by

$$G = \frac{E}{2\left(1 + \nu\right)} \tag{19}$$

where $\nu = 0.5$, signifying an incompressible material.

In our simulations, we fully constrained the bottom of the model. A 5% shear strain was applied to the top of model while preventing axial displacement. Figure 5 provides a schematic representation of the FE simulation, as well as the direction of the applied shear displacement and resulting forces. The results of the simulation are shown in Figures 6(a) and (b) in terms of F versus κ and α versus κ, respectively.

Further, in order to highlight the differences between the linear and nonlinear model, we conducted simulations while not constraining the model in the axial direction. Figure 7 shows the results the undeformed (solid line) versus deformed bodies for the linear and nonlinear elastic models for 5% shear strain. As seen in the figure, due to application of a shear displacement to the linear elastic model, only deformation in the transverse (along the direction of shear) is seen. But for the nonlinear elastic model, there is deformation in the transverse as well as the axial direction, due to the Poynting effect. The displacement in the axial direction for the nonlinear elasticity-based model was found to be 8.6 mm.

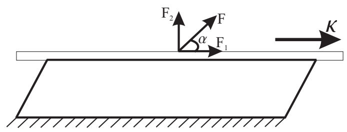

Figure 5. Direction of forces for the simple shear case, with $\alpha = \tan^{-1}\left(\frac{F_2}{F_1}\right)$ and $F = \sqrt{F_1^2 + F_2^2}$

5. Discussion

For a wide variety of conditions, the Just Noticeable Difference (JND) for contact force in humans is approximately 7% [10]. Based on our simulation studies, as seen in Figure 6(a), the percentage change in magnitudes of the maximum reaction forces between the linear and nonlinear models is 51.2%, which is much greater than the JND. In Figure 6(b), the angle between the reaction forces in the transverse and

Second Joint EuroHaptics Conference and Symposium on Haptic Interfaces for Virtual Environment and Teleoperator Systems (WHC'07)
0-7695-2738-8/07 $20.00 © 2007 IEEE

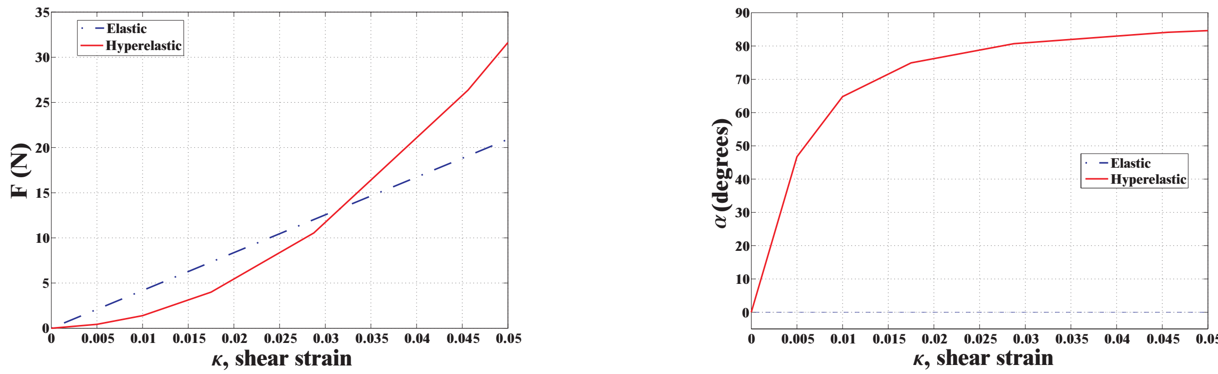

(a) (b)

Figure 6. FEM simulation results for (a) F versus κ (b) α versus κ. For 5% shear strain, the maximum values of F and α are 20.9 N and $0°$, and 31.6 N and $84.6°$, for linear and nonlinear (hyperelastic) models, respectively.

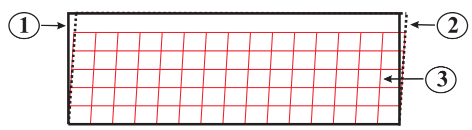

Figure 7. FEM simulations for 5% shear strain where ①, ②, and ③ represents the undeformed body, deformed body based on linear elasticity, and deformed mesh for the nonlinear elastic model, respectively. For these simulation cases, the model was not constrained axially while being sheared; the material coefficients correspond to sample #5 in Table 1. The coarse meshes in this figure are only presented for clarity, and were not used for analysis.

axial directions was found to be $84.6°$, while for the linear elastic model, since the Poynting effect is not observed, there is no normal reaction force for shear displacement. In [11], the mean force direction-discrimination thresholds were found to be $25.6°$ and $18.4°$, for haptic feedback and haptic feedback with congruent vision, respectively. This implies that, without the implementation of a nonlinear elastic tissue model in the surgical simulator, the user will receive noticeably different haptic feedback while interacting with the organ model. Further, preliminary sensitivity analysis has shown that decreasing both the Mooney-Rivlin material parameters by $\sim 40\%$ caused the angle between the reaction forces to increase by $\sim 15\%$. Also, though our study considered non-invasive surgical procedures, the results of this study are also applicable to invasive surgical procedures like needle insertion, where organs have asymmetric and complex boundary conditions, and shearing of tissue is common.

Part of the future work of this study entails conducting tests on human organs and comparing the results with that of animals and gels. We wish to use human tissues for building our simulation model because animal tissues, such as bovine or porcine liver, commonly used in the tissue modeling literature may have elastic properties different from human tissues. In this study, we used experimental data from samples undergoing $\sim 5\%$ strain. It is probably beneficial to fit material parameters for data collected over larger ($\sim 50\%$) strains. Hence, we plan to conduct shear tests on the RSA II using a specialized shear fixture. This would help us to apply larger strains and compare our simulation and experimental results. Moreover, in order to have greater confidence in our results, we are currently developing a setup to conduct large scale shear experiments using a 3-axis robot. In this study, the size of the gel sample would be comparable to actual organ dimensions. As the gel sample is sheared, the resulting forces would be recorded and compared with FE simulations.

A fundamental, yet unanswered, research question is what the fidelity of a surgical simulator should be so that realistic haptic feedback is provided to the user. Some researchers evaluate simulator effectiveness using “expert” surgeon subjective evaluation, while others test the ability of trainees to perform real (usually animal) surgeries before and after using the simulator. We propose a different approach, in which we model the flow of information from the real tissue to acquired data, the model, the rendering technique, the haptic and/or visual display, and eventually the human user (Figure 8). We conjecture that each of these stages acts as a “filter” in which information about force-motion relationships are lost or transformed. For example, the filter may be a result of the resolution of the measurement device used for gathering experimental data, the simulation model based on the constitutive law derived from experimental data, or simplification of the model required to perform real-time haptic rendering. In addition, haptic devices have their own dynamics and are affected by control issues such as sample-and-hold and quantization. Finally, human perception plays an vital role in quantifying

Second Joint EuroHaptics Conference and Symposium on Haptic Interfaces for Virtual Environment and Teleoperator Systems (WHC'07)
0-7695-2738-8/07 $20.00 © 2007 IEEE

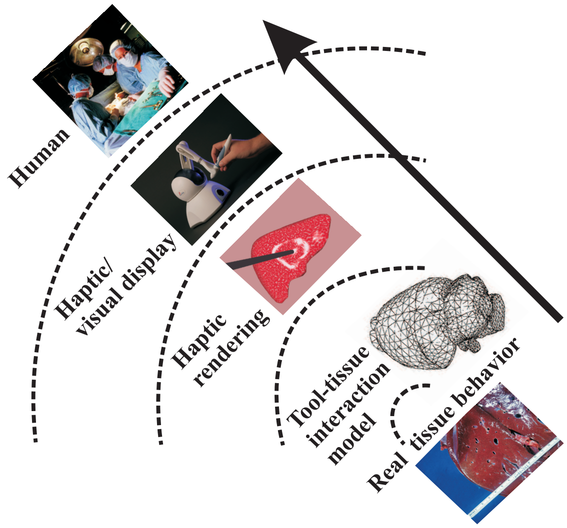

Figure 8. The modeling of force flow in order to quantify the amount of force felt by the human.

the necessary fidelity of the simulation. In this paper, we have presented an example scenario, where the filter is the modeling technique. We showed that, in comparison to the human filter, the effect of the fundamental tissue modeling technique is significant.

Acknowledgments

The authors would like to thank Dr. Shailendra Joshi and Scott Decker for their help in the FE simulations and tests on the RSA II, respectively. This research was supported by NSF Grant No. EIA-0312551 and NIH Grant No. R01-EB002004.

References

[1] M. Bro-Nielsen. Finite element modeling in surgery simulation. *Proc. IEEE*, 86(3):490–503, 1998.

[2] E. Dehghan and S. E. Salcudean. Comparison of linear and mon-linear models in 2d needle insertion simulation. In *Computational Biomechanics for Medicine:9th MICCAI Conf. Workshop*, Oct. 2006.

[3] S. P. DiMaio and S. E. Salcudean. Interactive simulation of needle insertion models. *IEEE Trans. Biomedical Engineering*, 52(7):1167–1179, 2005.

[4] Y. C. Fung. *Biomechanics: mechanical properties of living tissues*. Springer-Verlag Inc., New York, USA, second edition, 1993.

[5] S. F. Gibson and B. Mirtich. A survey of deformable modeling in computer graphics. Tech. Report TR-97-19, Mitsubishi Electric Information Technology Center America, Nov. 1997.

[6] M. E. Gurtin. *An introduction to continuum mechanics*. Academic Press, London, UK, first edition, 2003.

[7] T. Hu and J. P. Desai. Characterization of soft-tissue material properties: large deformation analysis. In S. Cotin and D. N. Metaxas, editors, *Proc. Medical Simulation: Int'l Symp.*, volume 3078 of *Lecture Notes in Comp. Science*, pages 28–37. Springer, Berlin/Heidelberg, 2004.

[8] D. James and D. K. Pai. A unified treatment of elastostatic contact simulation for real time haptics. *Haptics-e*, 2(1):1–13, 2001.

[9] H.-W. Nienhuys and F. A. van der Stappen. A computational technique for interactive needle insertions in 3d nonlinear material. In *Proc. IEEE Int'l. Conf. on Robotics and Automation*, pages 2061–2067, May 2004.

[10] M. A. Srinivasan and J.-S. Chen. Human performance in controlling normal forces of contact with rigid objects. In *Proc. ASME Dynamic Systems and Control Division*, pages 119–125, Nov.-Dec. 1993.

[11] Barbagli et al. Haptic discrimination of force direction and the influence of visual information. *ACM Trans. Applied Perception*, 3(2):125–135, 2006.

[12] Basdogan et al. Virtual environments for medical training: Graphical and haptic simulation of laparoscopic common bile duct exploration. *IEEE/ASME Trans. Mechatronics*, 6(3):269–285, 2001.

[13] Carter et al. Measurements and modelling of the compliance of human and porcine organs. *Medical Image Analysis*, 5(4):213–236, 2001.

[14] Cotin et al. Real-time elastic deformations of soft tissues for surgery simulation. *IEEE Trans. Visualization and Computer Graphics*, 5(1):62–73, 1999.

[15] Delingette et al. A craniofacial surgery simulation testbed. In *Proc. 3rd Int'l. Conf. on Visualization in Biomedical Computing*, pages 607–618, Oct. 1994.

[16] E. Molinari et al. Simulation of the biomechanical behavior of the skin in virtual surgical applications by finite element method. *IEEE Trans. Biomedical Engineering*, 52(9):1514–1521, 2005.

[17] Kerdok et al. Truth cube: Establishing physical standards for soft tissue simulation. *Medical Image Analysis*, 7(3):283–291, 2003.

[18] Kühnapfel et al. Endoscopic surgery training using virtual reality and deformable tissue simulation. *Computers and Graphics*, 24(5):671–682, 2000.

[19] Picinbono et al. Anisotropic elasticity and force extrapolation to improve realism of surgery simulation. In *Proc. IEEE Int'l. Conf. on Robotics and Automation*, pages 596–602, Apr. 2000.

[20] Picinbono et al. Non-linear anisotropic elasticity for real-time surgery simulation. *Graphical Models*, 65(5):305–321, 2003.

[21] Rheometerics Solids Analyzer RSAII Owner's Manual. Tech. Report 902-00013A, Rheometrics Inc., Dec. 1991.

[22] Sedef et al. Visual and haptic simulation of linear viscoelastic tissue behaviour based on experimental data. In *Proc. 14th Symp. on Haptic Interfaces for Virtual Environments and Teleoperator Systems*, pages 201–208, Mar. 2006.

[23] Sundaraj et al. A fast method to simulate virtual deformable objects with force feedback. In *7th Int'l Conf. on Automation, Robotics, Control, and Vision*, pages 413–418, Dec. 2002.

[24] Székely et al. Virtual reality-based simulation of endoscopic surgery. *Presence: Teleoperators & Virtual Environments*, 9(3):310–333, 2000.

[25] W. Wu and P. A. Heng. An improved scheme of an interactive finite element model for 3d soft-tissue cutting and deformation. *The Visual Computer*, 21(8-10):707–716, 2005.

[26] H. Yamada. *Strength of biological materials*. The Williams & Wilkins Company, Baltimore, USA, first edition, 1970.